Excitonic transitions in GaAs/$Ga_xAl_{1-x}As$ quantum wells observed by photoreflectance spectroscopy: Comparison with a first-principles theory

W. M. Theis
University Research Center, Wright State University, Dayton, Ohio 45435

G. D. Sanders
Universal Energy Systems, 4401 Dayton-Xenia Road, Dayton, Ohio 45432

C. E. Leak and K. K. Bajaj
Avionics Laboratory, U.S. Air Force Wright Aeronautical Laboratories (AFWAL/AADR), Wright-Patterson Air Force Base, Ohio 45433

H. Morkoç
Department of Electrical Engineering and Coordinated Science Laboratory, University of Illinois at Urbana-Champaign, Urbana, Illinois 61801

(Received 17 August 1987)

Excitonic transitions in GaAs-$Al_xGa_{1-x}As$ multiple quantum wells are observed using photoreflectance spectra obtained with a novel double-monochrometer spectrometer. The first pass of the monochrometer produces the infrared probe beam while the second pass is used as a synchronous band-pass filter, resulting in a better signal-to-noise ratio than the low-pass filter conventionally used, and allowing simultaneous collection of the photoluminescence spectrum. The photoreflectance data are analyzed using a multiband effective-mass theory which includes valence-band mixing and assumes a first-derivative modulation of the built-in field as the dominant modulation mechanism. The entire photoreflectance spectrum is simultaneously fit using a first-principles theory in which only the exciton linewidth and value of the built-in electric field are not determined by the theory. Full advantage is thus taken of the signal intensity information, in contrast to comparisons currently encountered in the literature where positions of excitons are usually compared to values predicted by a finite-square-well calculation, without valence-band mixing effects. The theory is shown to have much success in explaining the observed photoreflectance signal from a 200-Å multiple quantum well at 77 K, including the qualitative line shape for any given exciton.

I. INTRODUCTION

Photoreflectance spectroscopy (PR) performed at room temperature has recently been shown to be an accurate method for the characterization of multiple-quantum-well (MQW) structures.[1,2] Specifically, this technique measures the energies of excitonic transitions confined in the MQW, which may then be interpreted in terms of well dimensions, barrier heights, interfacial quality, and so forth. Although it is possible to obtain this information by other techniques, the comparative ease and accuracy of PR at room temperature have established it as a convenient tool for MQW characterization. In comparison, photoluminescence (PL) and resonant Raman spectroscopies are frequently performed at cryogenic temperatures, transport-related techniques (i.e., photocurrent spectroscopy) require contacts, and infrared absorption requires a window to be etched through the substrate so the MQW alone may be measured. Even electroreflectance spectroscopy (ER), a closely related technique, requires the sample either be placed in an electrolytic solution or have electrical contacts formed for application of an external electric field. PR, which involves modulation of the built-in electric field by chopping a pump light beam, has the advantage of being contactless and therefore nondestructive. Additionally, the possibility of performing convenient lateral profiling exists.

To exploit fully the information obtained from PR, an understanding of the underlying modulation mechanisms is necessary. An important step towards this understanding was made by Shanabrook *et al.*,[3] who compared the results of photoluminescence excitation spectroscopy (PLE) with PR measurements made on MQW's at low temperature (4 K). One conclusion of this study was that interband excitonic, rather than band-to-band transitions, dominate the PR effect in MQW's even at room temperature and that the change in reflectance occurs due to modulation of the dielectric function through changes in the exciton transition energy, lifetime, and oscillator strength. This conclusion is in agreement with results from other techniques[4–9] and contrasts with previous interpretations for ER in bulk semiconductors where the Franz-Keldysh effect for a

two-dimensional critical point (band-to-band transition), as described by the third-derivative functional form (TDFF), is typically used.[10] Another study[11] comparing PLE to ER in MQW's confirms that ER is like PR in that the features in the spectra arise from excitonic effects rather than the Franz-Keldysh effect. A recent study has shown that application of TDFF to PR of MQW is physically inappropriate but sufficiently mimics the excitonic description to produce line shapes that are essentially indistinguishable from the excitonic formulation at room temperature.[12] Furthermore, this study found that the excitonic line shape in absorption changes from Gaussian character (at room temperature) to Lorentzian as temperature is reduced below about 150 K. If a Kramers-Kronig conversion is performed on the imaginary part of the dielectric function (which determines the absorption line shapes) to obtain the real part (which dominates PR line shapes), this change in character qualitatively describes the observed line shapes in PR as a function of temperature.

This paper attempts to refine the conclusions of Shanabrook *et al.*[3] by exploiting a quantitative first-principles theory to calculate the variation of the exciton energy gap and oscillator strength due to changes in the electric field, and appropriately apply these variations to the interpretation of the physical processes involved in PR or ER. The basis for this work is a multiband effective-mass theory of quantum wells in an electric field.[13] After estimating the built-in electric field, the experimentally measured linewidths for each exciton are incorporated into a calculation of the PR signal, ignoring the exciton linewidth modulation mechanism which is expected to be negligible for the lowest-lying excitonic features.[3] This results in an artificial PR spectrum which has *no* fitting parameters and which may then be compared to experimental spectra. With these starting values a least-squares fit may be attempted by allowing the linewidths to vary. Furthermore, it is possible to introduce another fitting parameter, the derivative of the exciton linewidth with respect to the built-in electric field, which is not determined either by the theory or experiment. The experimental data used in these fits were low-temperature PR spectra of extremely high interfacial quality MQW's, taken with sufficient resolution to resolve adequately the line shapes of each feature. The combination of simultaneously having the multiband effective-mass theory and the best possible experimental data allowed a definitive test of the theory as well as the investigation of many physically important effects, such as the quantum-confined Stark shift and its implications for PR.

II. THEORY

Before embarking upon a formal discussion of the theory used in this paper, it is necessary to consider the very complicated physical processes involved in the PR measurement. Although the following discussion assumes a p-type (uniform) doping throughout the entire structure, the extension to n-type doping is easily made. For unintentionally doped layers grown by molecular-beam epitaxial (MBE) techniques such as those of this study, p-type doping is usually the case due to background carbon acceptors. Since the pump beam is modulated very slowly compared to free-carrier and excitonic lifetimes, all transient behavior in the MQW's may be ignored. In the PR measurement, the signal is proportional to the change in the reflected probe beam which is responding to changes in the dielectric function of the sample due to the pump beam being on or off. For the pump-beam-off case, there is an electric field due to the pinning of surface states making a total band bending of ϕ and producing a surface depletion region (SDR). The maximum value of the associated built-in electric field $F_{\rm BI}$ is crudely given by $(2eN_d\phi/\epsilon)^{1/2}$ where N_d is the uniform doping density, e the charge of an electron, and ϵ the dielectric constant. Due to the presence of the MQW's, the expression for $F_{\rm BI}$ versus distance from the sample surface is complicated. In addition to the SDR, there are small depletion regions formed at each interface of the MQW's due to charge transfer from the $Al_xGa_{1-x}As$ barriers into the GaAs wells. The extent of these latter regions will be modulated by the pump beam but the effects on PR are expected to be insignificant, primarily because only a fraction of the volume of the MQW is subjected to the associated electric fields. This same argument also holds for any depletion region at the interface between buffer and MQW. Although the electric field experienced by any particular MQW could be estimated by solving a Poisson equation utilizing the distribution of space charges in the sample, the approximation is made that $F_{\rm BI}$ does not vary appreciably in the MQW's.

The impact of the photogenerated carriers on the dielectric function when the pump beam is on will be considered next. The field $F_{\rm BI}$ arising from the built-in potential causes photogenerated holes to drift towards the sample surface and neutralize the surface states thus reducing ϕ and creating a decrease in the field, as well as a decrease in the extent of the SDR. The photogenerated electrons will likewise move away from the surface. Free carriers formed in the vicinity of (or within) the MQW may become confined in the wells, where they either recombine or form excitons. The electric fields involved are insufficient to ionize the excitons in the MQW's but the excitons formed are polarizable and thus will tend to further diminish the built-in electric field, eliminating the necessity for holes to completely reach the surface to neutralize ϕ. The excess carriers will produce a sizable exciton population in the MQW's and GaAs buffer as compared with the pump-beam-off case. The presence of excitons has little impact on the dielectric function other than the fact that the linewidth of the observed PR features, as measured by the probe beam, depends on the recombination time of the exciton which, in the absence of interfacial broadening mechanisms,[14] depends on the radiative recombination rate.[15] Hence, the PR signal does *not* rely upon the *probe* beam exciting an excitonic transition but rather is the response of the probe beam to the existing dielectric function formed by the pump beam. Therefore, the decay lifetime rather than absorption time (which may be extremely short) is appropriate for the description of the PR process. The

probe beam cannot perturb the PR signal appreciably since it is so much less intense than the pump beam and furthermore is not modulated. Thus *one* of the effects of applying the pump beam, which impacts the excitonic properties (i.e., binding energy, lifetimes, etc.),[16,17] is a reduction in the electric field experienced by the MQW. This is equivalent to the surface photovoltaic effect and we shall assume that it is the dominant PR modulation mechanism. Thus the PR effect in MQW's must be accounted for by modulation of a dielectric function which includes excitonic contributions.[3] (This conclusion is further supported by the fact that energy locations of the PR features correspond to those for excitons as measured by PLE.) Furthermore, excitonic effects are expected to dominate even at higher temperatures, owing to the increased binding energy due to confinement. Such effects have already been observed in room-temperature absorption spectra of quantum wells.[4–9]

A number of other effects that can potentially modulate the dielectric function, and thus be of consequence to PR, have been proposed. An exciton screening modulation mechanism[18] has been proposed for bulk samples, which is subtly different from what we believe is the situation for MQW's. This treatment assumes that the excess carriers produced when the pump beam is on reduce the exciton concentration by free-carrier screening. This model is in contrast to the situation just described since the exciton population in the MQW's is actually significantly increased (rather than decreased) by turning on the pump beam. It was further concluded on the basis of the temperature dependence that the exciton screening modulation was not dominant in bulk GaAs. There is also a sample heating effect due to the application of the pump beam, which presumably could cause a thermoreflectance modulation.[19] However, the combination of low pump power and immersion in liquid He is expected to limit the contribution of this effect. Another study[3] (which also concluded that the exciton screening and sample heating modulations are insignificant) pointed out that for the pump beam intensities investigated, the number of estimated free carriers produced is not sufficient to create significant renormalization of the exciton energy gap due to many-body effects. Electric field quenching of the excitons in the MQW is not likely to be important in light of the enhancement of the excitonic binding energy due to confinement[20] and in light of the small size of the built-in field. The creation of a Dember potential[17] or transverse photovoltage, also proposed to account for the modulation in bulk semiconductors, relies upon producing a diffusion current from the photoexcited carriers. Due to difference in electron and hole diffusion constants a space charge is produced in response to the pump beam creating a transverse voltage. The usual formalism of the Dember potential estimates the transverse voltage arising between the illuminated and dark (front and rear) surfaces of the sample but does not account for charge trapping due to the MQW's, which would certainly occur. If, however, the Dember potential were to be the dominant mechanism it would be expected to produce electric fields upon application of the pump beam and would thus produce PR spectra of opposite sign to that predicted on the basis of SDR electric field modulation, which diminishes the electric field upon application of the pump beam. The other significant difference would be that the Dember potential should not show saturation effects. The SDR modulation, on the other hand, saturates once the pump beam is of sufficient intensity to produce flat-band conditions (complete neutralization of the SDR by photogenerated free carriers) so that there can be no further signal enhancement with additional intensity. The latter is the experimentally observed situation[3] which conclusively demonstrates that the Dember potential is not significant in the MQW's investigated. Band-filling effects[21] might produce a PR response from the region of the sample within the penetration depth of the pump beam, which may be greater than the SDR, especially when heavily doped cladding layers are present. However, the observation that neutralizing the built-in field causes PR in bulk materials to vanish argues strongly in favor of the notion that neutralization of the SDR is the dominant modulation mechanism in MQW's, since these other mechanisms are essentially independent of these space-charge fields.[17] Therefore, until future experimentation is able to conclusively discern the dominant modulation mechanism for MQW's the present treatment of using the reduction in the built-in field and its effects on the dielectric function to predict the PR response is presumed to be valid.

Our formal theory of ER and PR spectroscopy in MQW's is based on a multiband effective-mass theory of quantum wells in an electric field, which successfully accounts for light- and heavy-hole mixing in the valence band. For quantum wells we believe, for reasons mentioned above, that the ER or PR spectrum is due to electric field modulation of the excitonic transitions rather than band-to-band transitions as in bulk semiconductors. The electric field modulation of the dielectric function is related to the normalized change in the reflectivity, $\Delta R/R$, measured in ER and PR experiments by[22]

$$\Delta R/R = (1/R)[(\delta R/\delta\epsilon_1)\Delta\epsilon_1 + (\delta R/\delta\epsilon_2)\Delta\epsilon_2] \equiv \alpha\Delta\epsilon_1 + \beta\Delta\epsilon_2 \ . \quad (1)$$

In the above expression $\alpha(\epsilon_1,\epsilon_2)$ and $\beta(\epsilon_1,\epsilon_2)$ are the Seraphin coefficients, and $\epsilon_1(\hbar\omega)$ and $\epsilon_2(\hbar\omega)$ are the real and imaginary parts of the dielectric function ϵ, respectively, with $\Delta\epsilon_1$ and $\Delta\epsilon_2$ being the changes due to modulation by the electric field. Although this expression was originally derived for the case of band-to-band transitions, it is applicable to the situation in MQW's provided that the proper dielectric function ϵ, containing an excitonic component as well as the usual band-to-band component, is used. The effect is an admixture of the $\Delta\epsilon_1$ and $\Delta\epsilon_2$, particularly in the vicinity of the strongest excitons. The ER line shapes are known[22] to be affected by changes in the sign of β or crossover of α and β (the $\hbar\omega$ for which $\beta > \alpha$). The approximation of $\beta \approx 0$ made by Shanabrook *et al.*[3] is equivalent to assuming that $\Delta R/R$ is entirely determined by $\Delta\epsilon_1$. In our study, this assumption was relaxed by calculating β as a function of energy and assuming α to be constant. Using the ab-

sorption coefficient (which is proportional to $2\omega k/c$) generated by the multiband effective-mass theory including the band-to-band and excitonic contributions,[13] ϵ_2 was determined. The relationship of ϵ to the index of refraction (n) and the extinction coefficient (k) is $\epsilon_1 \equiv n^2 - k^2$ and $\epsilon_2 \equiv 2nk$. Since n is essentially constant [$n \approx 3.4$ to within 1% even in the presence of the MQW's (Ref. 23)], $\epsilon_1 \approx n^2 = 11.56$ since $n \gg k$ for all $\hbar\omega$ of interest. Using ϵ determined in this manner, the energy dependence of $\beta(\hbar\omega)$, including excitonic effects, was obtained for several sizes of MQW's. As a further check on our calculation, a treatment[23] which includes the variation in n but neglects valence-band mixing was used to compute α and β as a function of energy. This calculation yields an α constant to within $\pm 4\%$ and a β similar to the one calculated using the multiband effective-mass theory, further justifying our approximations. The effects of including nonzero β on the PR line shapes will be discussed later in this paper.

Following Shanabrook *et al.*[3] we assume the bound excitonic transitions at low temperatures exhibit a Lorentzian or Gaussian absorption profile and that band-to-band contributions are negligible in comparison. We then obtain the reflectance spectrum by summing over contributions from the various bound excitonic transitions.[3] Thus $\Delta R/R(\hbar\omega)$ is

$$\Delta R/R = \sum_{n,m} [\alpha(\Delta\epsilon_1)_{n,m} + \beta(\Delta\epsilon_2)_{n,m}] \ . \tag{2}$$

The contribution of any particular exciton can be expanded as the sum of three electric-field-modulated components:[3]

$$\begin{aligned} d(\epsilon_1)_{n,m} &= [(\delta\epsilon_1/\delta E_{n,m})(\delta E_{n,m}/\delta F) + (\delta\epsilon_1/\delta f_{n,m})(\delta f_{n,m}/\delta F) + (\delta\epsilon_1/\delta\Gamma_{n,m})(\delta\Gamma_{n,m}/\delta F)]dF \ , \\ d(\epsilon_2)_{n,m} &= [(\delta\epsilon_2/\delta E_{n,m})(\delta E_{n,m}/\delta F) + (\delta\epsilon_2/\delta f_{n,m})(\delta f_{n,m}/\delta F) + (\delta\epsilon_2/\delta\Gamma_{n,m})(\delta\Gamma_{n,m}/\delta F)]dF \ , \end{aligned} \tag{3}$$

which are due to variations of the exciton transition energies ($E_{n,m}$), oscillator strengths ($f_{n,m}$), and Lorentzian full widths at half maximum ($\Gamma_{n,m}$) due to changes in the built-in electric field. dF is the magnitude of the modulation of the built-in electric field F. (In ER experiments dF is due to an ac modulation of the applied voltage. In PR experiments dF is due to the modulation of the built-in field via screening by photoexcited carriers, as described above.) The assumption of strong exciton-phonon coupling at low temperatures yields a Lorentzian excitonic line shape which can be incorporated by using a dielectric function,[24]

$$\begin{aligned} \epsilon_L(E) &= \epsilon_1 + i\epsilon_2 \\ &= (1/\pi) \sum_{n,m} (-f_{n,m})/(E - E_{n,m} + i\Gamma_{n,m}) \ , \end{aligned} \tag{4}$$

which allows expressions for $\delta\epsilon/\delta E_{n,m}$, $\delta\epsilon/\delta f_{n,m}$, and $\delta\epsilon/\delta\Gamma_{n,m}$ to be obtained in closed form. In the above expressions the indices (n,m) refer to the nth conduction subband and mth valence subband. (By convention, if $n = m$ the extra index is dropped, thus making 1H the notation used for the lowest-lying exciton composed of the $n = 1$ electron and $m = 1$ heavy hole. The lowest-energy light-hole exciton is likewise 1L.) Application of this formalism to high-temperature PR and ER spectra (the weak exciton-phonon coupling limit or inhomogeneous broadening due to well width variation) requires substitution of a functional form which exhibits a Gaussian absorption profile for the exciton.[12] Such an analysis leads to PR and ER line shapes involving hypergeometric functions,[25] $\Phi(z)$, yielding

$$\begin{aligned} \epsilon_G(E) = (1/\pi) \sum_{n,m} & (-f_{n,m}/b\Gamma_{n,m}) \\ & \times [-x_{n,m}\Phi(x_{n,m}^2) + i\pi^{1/2}/2] \\ & \times \exp(-x_{n,m}^2) \ , \end{aligned} \tag{5}$$

where

$$x_{n,m} \equiv (E - E_{n,m})/(2b\Gamma_{n,m}) \tag{6}$$

and

$$\Phi(z) \equiv \frac{1}{\sqrt{2}} \int_0^{\sqrt{2}} \exp(zt^2/2)dt \ . \tag{7}$$

The normalization for both ϵ_L and ϵ_G is selected so that the integration of ϵ_2 for the (n,m)th exciton (which is proportional to the absorption) over all E for either function yields $f_{n,m}$. The constant b in ϵ_G is $1/(2\sqrt{\ln 2})$ and is included so that the full width at half maximum (FWHM) for the Gaussian matches that of the Lorentzian function. [The FWHM of ϵ_2 is 2Γ in Eq. (4) and is $4b\sqrt{\ln 2}\Gamma$ in Eq. (5).] The above conventions were chosen so that it is possible to account for admixtures of Lorentzian and Gaussian characters in the exciton line shape by approximating the total line shape by

$$\epsilon = \eta\epsilon_L + (1-\eta)\epsilon_G \tag{8}$$

and with η being a fitting parameter determined by the best least-squares fit to the observed line shape. The linear combination of these line shapes in Eq. (8) approximates, to a high degree, the Voigt function,[26] which may be appropriate for intermediate exciton-phonon coupling.

To carry out the calculations indicated in Eqs. (2)–(8) from first principles one needs to be able to calculate $E_{n,m}$, $f_{n,m}$, and $\Gamma_{n,m}$ and their associated derivatives as functions of the electric field for all excitons. The determination of the above six quantities for each excitonic transition is simply an application of the theory of the quantum-confined stark effect (QCSE), which has received much attention in the literature in recent years.[27,28] The importance in ER of the QCSE on excitons was realized and incorporated into the semiempiri-

cal approach of Klipstein and Apsley.[29] In that study, the ER line shape was formed by subtracting two Lorentzian-shaped exciton features in absorption whose optical transition energies were shifted by the QCSE as a result of an electric field applied perpendicular to the well. This result, which approximates the first-derivative nature of the ER, intentionally neglects modulation mechanisms other than $\delta R/\delta E_{n,m}$ and was therefore only applied to 1H and 1L where this is known to be the dominant mechanism. We have recently carried out a detailed study of excitonic QCSE in $GaAs/Al_xGa_{1-x}As$ quantum wells in which we calculated $E_{n,m}$ and $f_{n,m}$ as functions of F from a first-principles approach.[13] In that study we used a multiband effective-mass method which was based on an extension of the $\mathbf{K}\cdot\mathbf{P}$ method in bulk semiconductors to the case of thin films as first described by Nedorezov[30] and later used in the study of quantum-well structures by Fasolino and Altarelli.[31] We found that our computed electronic and optical properties were the result of an interplay between the effects of the overlap of electron and hole envelope wave functions and the mixing of valence subbands. Additional details on these calculations may be found in Ref. 13. Thus we have at our disposal a method of calculating four of the six quantities, per exciton, needed to implement the program of Eq. (3) from first principles. Of the remaining two quantities, $\Gamma_{n,m}$ and $\delta\Gamma_{n,m}/\delta F$, we can measure $\Gamma_{n,m}$ directly from the PR spectrum. The determination of $\delta\Gamma_{n,m}/\delta F$, however, is more problematic. The exciton linewidth is related to the exciton lifetime which may depend on three important effects: the tunneling lifetime for free carriers,[32] the details of interface roughness,[14] and the radiative recombination rate.[15] These effects are not easily incorporated into the present calculation. Time-resolved luminescence studies of high-quality $GaAs/Al_xGa_{1-x}As$ quantum wells at low temperature indicate that, at least for the lowest-lying heavy-hole exciton, the lifetime is determined by radiative recombination for the low values of F appropriate to the built-in fields encountered in PR experiments.[32] For these cases there is a drastic increase in the recombination lifetime as a function of increasing field, hence $\delta\Gamma_{n,m}/\delta F<0$ for the 1H exciton. For excitons of higher energy, however, one expects interface roughness and tunneling effects to become increasingly more important, and for these lifetime mechanisms $\delta\Gamma_{n,m}/\delta F>0$. Consequently, it is expected that $\delta\Gamma_{n,m}/\delta F$ may vary greatly, particularly for the lowest-lying excitonic transitions, so we shall treat it as a free parameter whose magnitude and sign are to be determined by the best least-squares fit to experimental data.

The details of the least-squares fit will now be considered. Our theory requires values for the conduction- and valence-band offsets between GaAs and $Al_xGa_{1-x}As$ (the value used was 60:40), the x value (determined by measuring the band edge of the $Al_xGa_{1-x}As$ via PR), the well dimensions (varied until agreement between experimental and theoretical exciton positions is achieved), the electron mass ($m^*=0.067m_e$, where m_e is the mass of a free electron), and values for the Kohn-Luttinger parameters ($\gamma_1=6.79$, $\gamma_2=1.92$, and $\gamma_3=2.81$, which produce hole masses $m^*_{HH}=0.34m_e$ and $m^*_{LH}=0.094m_e$). A value for the electric field due to the SDR must either be estimated or treated as a parameter. (We have found that the goodness of fit if fairly insensitive to the value of field F_{BI}, as compared to other parameters, and therefore an estimate is sufficient.) As stated above, $E_{n,m}$, $f_{n,m}$, and their respective derivatives with respect to F are then calculated with a choice of exciton line shape to produce an artificial PR spectrum. The standard least-squares criterion was employed (i.e., χ is equivalent to the square root of the sum of the squares of the differences between the theoretical and experimental spectra at each energy value normalized by the number of energy values). To account for the temperature dependence of the band gap, a global fitting parameter, dE, allowed movement of the entire artificial PR spectra in energy. Another global parameter, I, scaled the overall PR signal intensity to match theory and experiment to the least-squares criterion. Approximate starting values of $\Gamma_{n,m}$ for the nonoverlapping excitonic features (i.e., 1H and 1L) were determined by the criterion of Aspnes.[10] The value of χ was then minimized, using a simplex method, by variation of the $\Gamma_{n,m}$ and with the optional addition of $\delta\Gamma_{n,m}/\delta F$, η, or the value of F_{BI} due to the SDR as fitting parameters. While $\Gamma_{n,m}$ and $\delta\Gamma_{n,m}/\delta F$ are selected independently for each exciton, η and the built-in field F_{BI} are global parameters applied to the entire PR spectrum. Although it is physically possible that the values of $\Gamma_{n,m}$ may differ for each exciton, it is expected that excited states have $\Gamma_{n,m}$ greater than or equal to underlying ones. Applying this constraint reduced the number of parameters by allowing $\Gamma_{n,m}$ to vary only for excitons with large contributions to the PR signal and setting all higher excited states to a single value. It is worth pointing out that this is a different approach to comparison of theory to experiment than that currently in the literature. Rather than fit[33] positions of individual excitons using TDFF formalism and compare them to predicted ones (usually the results of a finite-square-well calculation without valence-band mixing effects), the entire PR spectrum is fit simultaneously, thus taking advantage of the signal intensity information. In this way it should be possible to estimate the values of such quantities as $\Gamma_{n,m}$ $\delta\Gamma_{n,m}/\delta F$, and η, as well as an approximate value for the build-in electric field.

III. EXPERIMENT

The PR spectra were obtained using a novel system based on a dual-pass monochrometer. A 650-W quartz halogen lamp supplies light to the first pass of the monochrometer to produce the monochromatic probe beam. This light is then channeled, using $f/\cdots$ matched optics, to the sample located in a variable-temperature Dewar vessel. The reflected light is collected into the

second half of the monochrometer, which is synchronously following the first. Consequently this behaves as an extremely selective band-pass filter which rejects all frequencies of light other than the one at which reflectance is being measured ($\hbar\omega$). The output of the analysis monochrometer is imaged onto a silicon detector whose modulated signal is analyzed by conventional lock-in techniques and digitized to obtain the change in reflectance $\Delta R(\hbar\omega)$. The dc level of the detector is also recorded, via digitization of an electrometer, to obtain the reflectance $R(\hbar\omega)$. $\Delta R/R$ is then obtained by digitally dividing the two signals. It should be noted that at low temperatures the modulated signal also contains a strong PL component so that $\Delta R+\text{PL}$ is the actual quantity measured. For these low-temperature cases the infrared beam from the first pass of the monochrometer may be blocked so that the PL component alone may be digitized. Consequently the $\Delta R/R$ spectrum is recovered by first subtracting the PL from the $\Delta R+\text{PL}$ and the normalizing with R. Note that in this way the PL spectrum is obtained as well, and can be used for comparisons to $\Delta R/R$ peak positions. Spectra were collected between 10 and 300 K with a typical resolution of 0.1 meV. The pump beam was either a 5-mW He-Ne (633 nm) or a 4-W Ar^+ (514.5 nm) laser which was modulated by chopping at 150 Hz and whose power density was varied via neutral density filters to explore power dependences of the PR line shapes. It was found that for the samples used in this study, power densities of 0.17–300. mW/cm^2 made essentially no difference in PR line shapes of the 1H and 1L excitons, although the intensity of these features varied approximately as the cube root of the laser power.

There are significant signal-to-noise advantages of using a second synchronous monochrometer as a band-pass filter rather than the low-pass filter which is conventionally employed in most PR systems. One advantage arises from better rejection of the pump beam, particularly when the sample surface is rough, causing greater scatter of the beam into the detector. Another advantage exists in the case of low-temperature measurements. Monochrometer systems employing the low-pass filter approach measure a ΔR which includes the *integrated* PL signal which is impossible to separate from the ΔR signal. It is usually assumed that this integrated PL signal is constant in $\hbar\omega$ and therefore may be subtracted. In practice, the PL dominates the modulated signal to such an extent as to mask completely the small $\Delta R(\hbar\omega)$ effects, making the signal of interest practically undetectable. Experimentally this problem necessitates using large dc offsets on the collection electronics to obtain the modulated portion of the signal resulting in severe drift difficulties. Furthermore, as $\hbar\omega$ of the probe beam is changed, the integrated PL changes, generating a PLE-like spectrum which contributes to the dc portion of the detector signal or $R(\hbar\omega)$. In fact, by employing a monochrometer to select a particular window, this PLE spectrum arising from the probe beam can be measured.[3] Thus there are added difficulties in producing a reliable $\Delta R/R$ spectrum due to this underlying PLE dependence which is not easily removed. All of these problems are overcome by the synchronous monochrometer system described herein.

The samples used in this study were MBE-grown MQW's of $Ga_{1-x}Al_xAs/GaAs$ with mole fraction (x) nominally 0.3. Well dimensions (L_z) for the four samples investigated were 90–200 Å with barrier width (L_b) of 100 Å. Due to limited sample availability, a direct determination of the appropriate line shape to be incorporated into the theory by substrate removal and measurement of the infrared absorption was not possible. These same samples were utilized in a high-resolution PL and reflectance study[34,35] which reported fine structure with individual exciton linewidths of the 1H and 1L transition as narrow as 50 μeV, which indicates the extremely high *microscopic* quality of the interfaces for these particular samples. For the $L_z=180$ Å sample, the energy spread of the individual excitons composing the 1H and 1L envelope were approximately 0.91 and 1.08 meV, respectively. Theoretical estimates of the amount of interface roughness consistent with this linewidth and energy spread imply that they arise from a two-monolayer change in well size with islands of order 20–80 Å.[34,35] Consequently, it is important to note that the PR spectra reported here, with resolution approximately equal to 0.1 meV, are incapable of completely resolving the PR response due to the individual excitons but rather measures the envelope. This envelope width of the excitons, which is due to interfacial microstructure, is not to be confused with the width arising from excitonic radiative or tunneling lifetimes which presumably control the widths of the individual excitons composing the envelope. It was experimentally determined that it is possible to resolve these components at the lowest temperatures and smallest pump intensities, but since it is not important to the present study, these results will be presented elsewhere. Therefore, in the remainder of this paper, the conclusions of theory will be tested against experimental conditions where these effects do not have a significant impact on the PR line shapes.

IV. DISCUSSION AND RESULTS

A previous investigation of modulation mechanisms for PR in MQW's (Ref. 1) based its identification of the dominant mechanism on qualitative comparison of experimental data to $\delta\epsilon_1/\delta E_{n,m}$, $\delta\epsilon_1/\delta f_{n,m}$ or $\delta\epsilon_1/\delta\Gamma_{n,m}$ using Eq. (4). It was concluded that $\delta\epsilon_1/\delta E_{n,m}$ is responsible for the 1H and 1L excitonic features whereas $\delta\epsilon_1/\delta f_{n,m}$ is responsible for the 12H feature. In addition, the contribution of $\delta\epsilon_1/\delta\Gamma_{n,m}$ was concluded to be negligible for these three excitonic transitions. This analysis is now extended since it is possible to calculate all of these quantities, except those involving Γ, from first principles using the theory described in the previous section which includes mixing of $\Delta\epsilon_1$ and $\Delta\epsilon_2$ via nonvanishing β. Based on the previous study, a least-squares fit was first attempted assuming that $\delta\epsilon/\delta\Gamma_{n,m}\equiv 0$ with the results shown in Fig. 1. The ex-

perimental data for a 200-Å MQW measured at 77 K are shown in Fig. 1(a). The lowest-energy feature ($\approx$1506 meV) arises from the GaAs buffer which is not included in the theory. We speculate that the reason the buffer appears in PR is that the overlayers of MQW's (including $Al_xGa_{1-x}As$) are transparent to the probe beam at this frequency and consequently this is analogous to a bulk GaAs PR measurement. The FWHM's as determined by the Aspnes criterion[10] from the data are 1.3±0.2 meV for 1H and 1.5±0.2 meV for 1L. For this example spectrum, the Gaussian line shapes provided a better fit ($\chi=171$ over the range 1.505–1.535 eV) than the Lorentzian ($\chi=198$). For both Gaussian and Lorentzian line shapes, the best parameters for FWHM are 1.6 meV for 1H and 1.2 meV for 1L. The Gaussian-based fit is shown in Fig. 1(b) with the transition energy (labeled E) and intensity (f) modulation components shown is Fig. 1(c). The Gaussian line shape, while reproducing the "dips" better than the Lorentzian line shape, fails to exhibit the sharpness of the peak of the 1H feature. On the other hand, the Lorentzian description (without $\delta\Gamma_{n,m}/\delta F$ parameters) did not account for the low-energy dip of the 1H feature [shown in Fig. 1(d)], suggesting that a combination of these line shapes is more appropriate. Therefore η in Eq. (6) was allowed to vary, resulting in a dominance of the Gaussian line shape ($\eta\approx0.6$) for the best least-squares fit of this sample at this temperature (not shown).

An attempt was made to determine whether Lorentzian line shapes could account for the PR line shape if additional physical effects were included so that Gaussian line shapes need not be introduced. To this end, a variety of assumptions were made, including the assumption of a distribution of well widths and/or a variation in the built-in electric field from well to well. The former was accomplished by calculating the artificial PR spectra for wells with monolayer L_z differences which were then summed with a weighted Gaussian distribution centered on the L_z value which gave the best positions for the excitonic features. For the latter, it was realized that the electric field associated with the built-in potential decays from a maximum value at the sample surface to zero at the end of the SDR. The artificial PR spectra were therefore generated for a series of quantum wells where the built-in field F was assumed to vary linearly from the surface (and consequently linearly with well position) and then summed to obtain the total PR spectrum. The PR spectrum thus obtained was not significantly different from one using the average F throughout the series of wells. Neither of these two enhancements to our model, either separately or together, were able to explain the low-energy dip when Lorentzian line shapes alone are used. Finally, the linewidth modulation mechanism ($\delta\epsilon/\delta\Gamma_{n,m}$), which was previously assumed to make a negligible contribution, was allowed to vary in order to explore its effect on the PR line shape. Only the lowest-energy excitons required any $\delta\Gamma_{n,m}/\delta F$ to produce a better fit. Specifically, 1H was fit with $\delta\Gamma_{n,m}/\delta F=-0.07$ meV/(kV/cm) and 1L was fit with $\delta\Gamma_{n,m}/\delta F=-0.03$ meV/(kV/cm), producing $\chi=116$ using only Lorentzian line shapes [Fig. 1(e)]. Although the fit gave the lowest χ of any combination of parameters, it does not conclusively establish these values of $\delta\Gamma_{n,m}/\delta F$, since this low χ may simply by the effect of adding an extra parameter to the fit. This amounts to a 7% narrowing of the 1H exciton upon application of the electric field, which will be very difficult to confirm by other measurements at these field values. The direction of this linewidth narrowing is consistent with what would be expected for a QCSE, where an increase in recombination lifetime occurs as the built-in electric field is increased, for the lowest-lying excitons. Best fits for

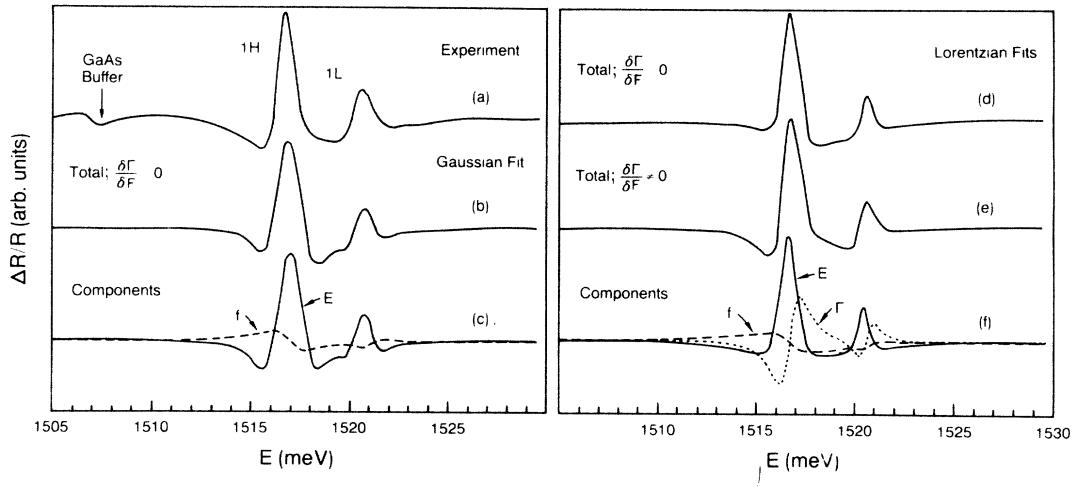

FIG. 1. Experimental and theoretical spectra for 1505–1530 meV of a 200-Å MQW at 77 K. (a) Experimental data. The GaAs buffer appears at approximately 1507 meV. (b) Theoretical result using Gaussian line shape with $\delta\Gamma_{n,m}/\delta F=0$ and FWHM=1.6 (1.2) meV for the 1H (1L) feature. (c) Transition energy (E) and intensity (f) components of Gaussian fit shown in (b). (d) Lorentzian fit with $\delta\Gamma_{n,m}/\delta F=0$ and FWHM same as Gaussian in (b). (e) Lorentzian fit with $\delta\Gamma_{n,m}/\delta F=-0.07$ (-0.03) meV/(kV/cm) for the 1H (1L) feature. (f) Transition energy (E), intensity (f), and linewidth (Γ) modulation components of Lorentzian fit shown in (e).

higher-energy excitons required that $\delta\Gamma_{n,m}/\delta F=0$. This is not surprising since these excitons are expected to have different $\delta\Gamma_{n,m}/\delta F$. The various components using Lorentzian line shapes due to transition energy (labeled E), intensity (f), and linewidth modulation (Γ) are shown in Fig. 1(f). Although the use of the linewidth modulation mechanism gives much better fits to the experimental data using Lorentzians and provides a means of obtaining the low-energy dip seen in the experimental data we believe that the Gaussian dependence is more appropriate since there is no necessity for nonvanishing $\delta\Gamma_{n,m}/\delta F$. If the $\delta\Gamma_{n,m}/\delta F$ are allowed to vary when using only Gaussian line shapes, the best least-squares fit occurs for small $\delta\Gamma_{n,m}/\delta F$ justifying the assumption of vanishing $\delta\Gamma_{n,m}/\delta F$ for MQW's. This may not always be the case since inhomogeneous broadening due to well width variation or well coupling (i.e., in a superlattice) might produce significant $\delta\Gamma_{n,m}/\delta F$.

Not determined by the theory is the magnitude of the electric field arising from the built-in potential, which was allowed to be determined by the best fit. This produced a value of approximately 3 kV/cm which is largely determined by the sensitivity to F of the relative intensities of the 1H and 1L exciton features as well as the 21H and 21L features.

The addition of effects due to nonzero β are fairly insignificant, justifying the assumptions of the previous work.[3] However, it is worth noting that for the 1H this contribution tends to produce a leading dip which assists in the explanation of the 1H feature in low-temperature PR data fit with Lorentzian line shapes. There was also a reduction of the 21H feature so that it more nearly corresponds to the observed PR signal. However, the size of the correction was insufficient to completely account for the observed spectra.

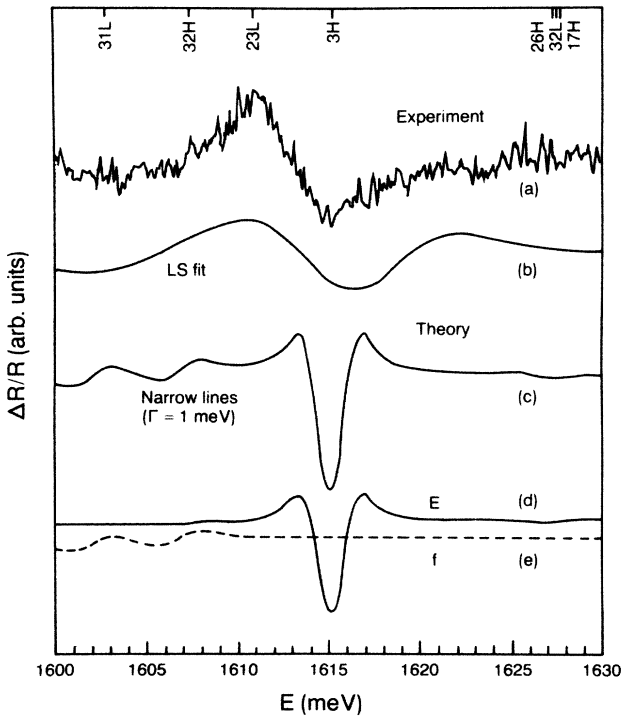

FIG. 2. Experimental and theoretical spectra for 1600–1630 meV of a 200-Å MQW at 77 K. (a) Experimental data. (b) Theoretical spectrum with $\Gamma_{n,m}$ least-squares fit using Gaussian line shape with $\delta\Gamma_{n,m}/\delta F=0$. (c) $\Gamma_{n,m}$ artificially narrowed to 1 meV to eliminate overlap of near-degenerate excitons (as labeled on top axis). (d) Transition energy (E) and intensity (f) components of Gaussian fit shown in (c).

An example of our analysis for one of the more complex higher-energy features is shown in Fig. 2. The positions of the various excitons calculated by the multiband effective-mass theory are labeled on the top axis of the figure. The experimental PR data in the range 1.6–1.63 eV is shown in Fig. 1(a) with the best least-squares (LS) fit in Fig. 2(b) for Gaussian line shapes with $\delta\Gamma_{n,m}/\delta F=0$. The contributions are shown (separated for clarity) for transition energy (E) and intensity modulation (f) in Figs. 2(e) and 2(f), respectively. Based on the energy of this feature and the dimensions of the well this feature would probably be identified as the 32H exciton by comparison with energy levels in a finite-square-well calculation. If, however, the linewidths of the excitons in our theoretical PR spectrum are artificially narrowed to 1 meV as shown in Fig. 2(c), the overlap of the various contributions is removed. Thus it is revealed that the dominant contribution is the energy-gap modulation of the 3H exciton with the 32H feature only adding a small low-energy shoulder. This indicates that care should be taken when assigning specific excitons to PR features on the basis of energy position information alone. Additionally, it shows that the contributions from the various modulation mechanisms determine the qualitative line shape for any given exciton. Consider, for example, the 3H exciton where the transition energy is predicted to *increase* with increasing electric field. This contrasts with the 1H exciton where transition energy *decreases* with increasing electric field. Consequently our theory predicts that the 1H and 3H excitons should produce features of opposite sign (transition energy modulation dominates both these excitonic features). This is indeed the case for the example spectrum studied here where the 1H feature is a "peak" in the PR spectrum whereas the 3H feature is a "dip."

It should be noted that the direction of the electric field in the presence or absence of the pump beam can be discerned by comparison of theory to experiment. Specifically, if theoretical spectra generated for $dF>0$ are in phase with the experimental data, then this would indicate an increase in electric field due to light present (Dember potential). On the other hand, if it is out of phase by a factor of -1 (peaks appear where dips are observed) then the electric field would be decreasing for light present, such as the case for reduction of the built-in field arising from the SDR. For the example spectrum the latter is the case, further demonstrating that modulation of the built-in field is the dominant modulation mechanism in PR. In making this judgement, care must be exercised in ensuring that interference effects,[29] which would also cause a change of phase factor, are properly treated. These effects may arise when cladding layers above the MQW's (overlayers) have a thickness

which is a significant portion of the wavelength of the reflected light. In this case, it is necessary to calculate the reflectivity of the entire structure using a multiple dielectric film approach. The samples used in the present study were specifically grown to minimize these effects (cladding layers less than 300 Å) so that the PR line shapes without these additional complications could be investigated. Further experimental study of these phase differences (Dember versus SDR) on a variety of samples over a range of temperatures are in progress.

In spite of all of these successes of the theory treating the PR mechanisms, certain discrepancies remain between theory and experimental PR spectra. In every case, the intensity of the 21H exciton is calculated to be noticeably larger than the observed size. By reducing the size of the built-in electric field in our theory the 21H transition may be diminished but never made as small as is necessary to explain the data. The remainder of the features appear to quantitatively agree, however, and explain a very complicated PR spectrum, as can be seen by comparing the experimental PR spectrum in Fig. 3(a) with a Gaussian line-shape fit of our theory with $\delta\Gamma_{n,m}/\delta F=0$ in Fig. 3(b) for excitons up to 34H. The components of the fit are shown separately for transition energy modulation (labeled E) in Fig. 3(c) and intensity modulation (f) in Fig. 3(d) and are separated for clarity. For the higher-energy excitons, the theory is expected to break down since tunneling reduces confinement of the electrons and holes.

A number of other possible modifications of the theory that were not incorporated will now be discussed. (a) No radical improvement in explaining the PR line shapes occurs when band-to-band effects due to the two-dimensional continuum are incorporated into the theory and are thus ignored in this paper. (b) Another potential description for the line shape not considered is the interaction of a discrete state with a continuum, as described by Fano.[36] For example, the 1L exciton, upon interaction with the 1H two-dimensional continuum, may be expected to be described by this line shape. A similar argument holds for all higher-energy excitons, each of which is resonant with a number of two-dimensional continua. This, however, is not the case for the 1H exciton whose binding energy lowers the energy position to below that of the onset of the 1H continuum. Consequently there is no continuum degenerate with the 1H exciton and the Fano description is inappropriate and cannot be invoked to explain the line shape of the 1H. (c) The "donor-related" feature previously reported[3] also appeared at the lowest temperatures (≈ 10 K) where the Lorentzian line shapes dominated. Presumably this feature is an impurity bound 1H exciton since it occurs at lower energy than the 1H free exciton. Thus the absence of this feature in the 77-K data is probably due to kT exceeding the disassociation energy of this center. (d) Interestingly, the effects of $\delta\Gamma_{n,m}/\delta F$ may be potentially calculated by our theory. The QCSE narrowing in principle can be accounted for in this theory by assuming radiative recombination lifetime and utilizing $\Gamma\equiv\Gamma_0|M_{cv}|^2=\Gamma_0\delta(\ln f_{n,m})/\delta F$ where Γ_0 is the individual excitonic linewidth in zero field, and M_{cv} is the overlap integral of the electron and hole wave functions which is given by the theory. However, the parameter Γ_0 is not the measured $\Gamma_{n,m}$ in the PR spectrum and would have to be treated as a fitting parameter. Therefore, no additional physical insight is gained whether Γ_0 or $\delta\Gamma_{n,m}/\delta F$ is used as the fitting parameter since neither choice leads to a reduction in undetermined parameters. Furthermore this treatment would ignore electric-field-induced increases in the exciton diameter within the plane of the layers which would further increase the lifetime of the individual exciton.

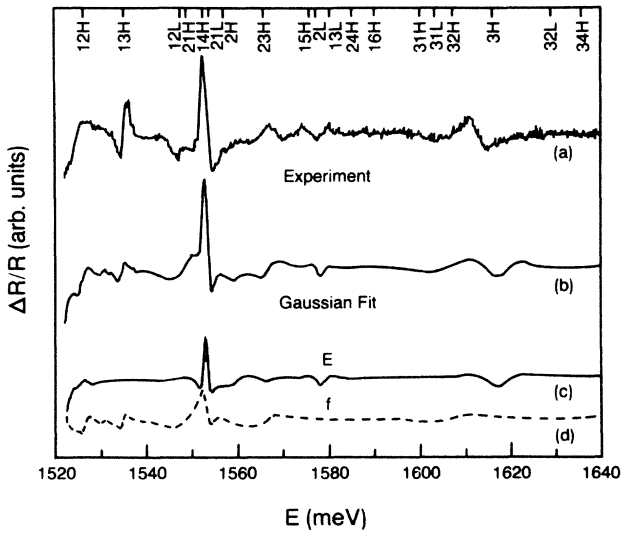

FIG. 3. Experimental and theoretical spectra for 1520–1640 meV of a 200-Å MQW at 77 K. (a) Experimental data. (b) Theoretical spectrum with $\Gamma_{n,m}$ least-squares fit using Gaussian line shape with $\delta\Gamma_{n,m}/\delta F=0$. (c) Transition energy (E) and (d) intensity (f) components of Gaussian fit shown in (b).

In conclusion, the multiband effective-mass theory which has been applied to PR spectra has had much success in explaining the observed low-temperature line shapes in a 200-Å MQW. After employing a reasonable guess for the built-in electric field and utilizing experimentally observed $\Gamma_{n,m}$, this first-principles theory has *no* fitting parameters (neglecting $\delta\Gamma_{n,m}/\delta F$) and provides reasonable agreement using either Lorentzian or Gaussian line shapes, as appropriate. The calculated spectra are not especially sensitive to the assumed size of the built-in electric field. A better fit is obtained if the $\Gamma_{n,m}$ are allowed to be determined by a least-squares-fit criterion. The same is true if $\delta\Gamma_{n,m}/\delta F$ or η (admixtures of Gaussian and Lorentzian line shapes) is included as a fitting parameter. It is not clear whether the values thus obtained for $\delta\Gamma_{n,m}/\delta F$ indicate a modest decrease of $\Gamma_{n,m}$ when small electric fields are applied or whether this represents solely a statistical improvement due to the addition of the extra fitting parameters. The effects of monolayer differences in L_z for the MQW or magnitude variation of the built-in electric field from well to well also were considered but found not to improve the agreement.

ACKNOWLEDGMENTS

This work was performed under U.S. Air Force Office of Scientific Research Contracts No. F33615-86-C-1062 and No. F33615-86-C-1050 at the Avionics Laboratory, Wright-Patterson Air Force Base Ohio. The authors would like to acknowledge the assistance of Yia-Chung Chang in providing a portion of computer code and helpful consultation. The authors would also like to thank Fred H. Pollak, and B. V. Shanabrook and O. J. Glembocki for useful discussions, and John Hoelscher for technical assistance.

[1]O. J. Glemboki, B. V. Shanabrook, N. Bottka, W. T. Beard, and J. Comas, Appl. Phys. Lett. **46**, 970 (1985).

[2]O. J. Glemboki, B. V. Shanabrook, N. Bottka, W. T. Beard, and J. Comas, in *Spectroscopic Characterization Techniques for Semiconductor Technology II,* edited by Fred H. Pollak [Proc. Sec. Photo-Opt. Instrum. Eng. **524**, 86 (1985)].

[3]B. V. Shanabrook, O. J. Glembocki, and W. T. Beard, Phys. Rev. B **35**, 2540 (1987).

[4]R. C. Miller, D. A. Kleinman, W. A. Norland, and A. C. Gossard, Phys. Rev. B **22**, 863 (1980).

[5]D. A. B. Miller, D. S. Chemla, D. J. Eilenberger, P. W. Smith, A. C. Gossard, and W. T. Tsang, Appl. Phys. Lett. **41**, 679 (1982).

[6]D. S. Chemla, T. C. Damen, D. A. B. Miller, A. C. Gossard, and W. Wiegmann, Appl. Phys. Lett. **42**, 864 (1983).

[7]P. Dawson, G. Duggan, H. I. Ralph, and K. Woodbridge, Phys. Rev. B **28**, 7381 (1983).

[8]D. S. Chemla, D. A. B. Miller, P. W. Smith, A. C. Gossard, and W. Wiegmann, IEEE J. Quantum Electron. **QE-20**, 265 (1984).

[9]D. A. B. Miller, D. S. Chemla, T. C. Damen, A. C. Gossard, W. Wiegmann, T. H. Wood, and C. A. Burrus, Phys. Rev. B **32**, 1043 (1985).

[10]D. E. Aspnes, Surf. Sci. **37** 418 (1973).

[11]P. C. Klipstein, P. R. Tapster, N. Apsley, D. A. Anderson, M. S. Skolnick, T. M. Kerr, and K. Woodbridge, J. Phys. C **19**, 857 (1986).

[12]O. J. Glemboki, B. V. Shanabrook, and S. Rudin, Bull. Am. Phys. Soc. **32**, 470 (1987).

[13]G. D. Sanders and K. K. Bajaj, Phys. Rev. B **35**, 2308 (1987).

[14]J. Singh, K. K. Bajaj, and S. Chaudhuri, Appl. Phys. Lett. **44**, 805 (1984).

[15]H.-J. Polland, L. Schultheis, J. Kuhl, E. O. Gobel, and C. W. Tu, Phys. Rev. Lett. **55**, 2610 (1985).

[16]F. Cerdeira and M. Cardona, Solid State Commun. **7**, 879 (1969).

[17]D. E. Aspnes, Solid State Commun. **8**, 267 (1967).

[18]W. Albers, Jr., Phys. Rev. Lett. **23**, 410 (1969).

[19]N. G. Nilson, Solid State Commun. **7**, 479 (1969).

[20]R. Enderlein, Phys. Status Solidi **26**, 509 (1968).

[21]J. G. Gay and L. T. Klauder, Phys. Rev. **172**, 811 (1968).

[22]B. O. Seraphin and N. Bottka, Phys. Rev. **145**, 628 (1966).

[23]Y. C. Chang, J. N. Schulman, and U. Efron, J. Appl. Phys. **62**, 4533 (1987).

[24]D. E. Aspnes and A. Frova, Phys. Rev. B **2**, 1037 (1970).

[25]See, for example, Eq. (9.211.1) in *Tables of Integrals, Series and Products,* edited by I. S. Gradshteyn and I. M. Ryzhik (Academic, New York, 1965).

[26]G. K. Wertheim, M. A. Butler, K. W. West, and D. N. E. Buchanan, Rev. Sci. Instrum. **45**, 1369 (1974); John F. Kelkopf, J. Opt. Soc. Am. **63**, 987 (1973).

[27]D. A. B. Miller, D. S. Chemla, T. C. Damen, A. C. Gossard, W. Wiegmann, T. H. Wood, and C. A. Burrus, Phys. Rev. B **32**, 1043 (1985).

[28]For a review of the quantum-confined Stark effect, see D. A. B. Miller, J. S. Weiner, and D. S. Chemla, IEEE J. Quantum Electron., **QE-22**, 1816 (1986), and references therein.

[29]P. C. Klipstein and N. Apsley, J. Phys. C. **19**, 6461 (1986).

[30]S. S. Nedorezov, Fiz. Tverd. Tela (Leningrad) **12**, 2269 (1970) [Sov. Phys.—Solid State **12**, 1814 (1971)].

[31]M. Altarelli, Phys. Rev. B **28**, 842 (1983); A. Fasolino and M. Altarelli, *Two Dimensional Systems, Heterostructures, and Superlattices* (Springer-Verlag, New York, 1984), p. 176.

[32]S. Hong and J. Singh, Appl. Phys. Lett. **49**, 331 (1986).

[33]H. Shen, P. Parayanthal, Fred H. Pollak, Micha Tomkiewicz, T. J. Drummond, and J. N. Schulman, Appl. Phys. **48**, 653 (1986).

[34]D. C. Reynolds, K. K. Bajaj, C. W. Litton, Jasprit Singh, P. W. Yu, P. Pearah, J. Klem, and H. Morkoç, Phys. Rev. B **33**, 5931 (1986).

[35]D. C. Reynolds, K. K. Bajaj, P. W. Yu, H. Morkoç, I. Shidlovski, K. Alavi, and C. Colvard, Appl. Phys. Lett. **46**, 51 (1985).

[36]U. Fano, Phys. Rev. **124**, 1866 (1961).